Development of a Reconfigurable Control Equivalent Turbulence Input Model for Multirotor UAS

Kevin V. Truong
Research Engineer
San Jose State University
Ames Research Center
Moffett Field, CA, USA

Anthony Gong
Aerospace Engineer
U.S. Army DEVCOM
Aviation & Missile Center
Moffett Field, CA, USA

Tom Berger
Flight Controls Group Lead
U.S. Army DEVCOM
Aviation & Missile Center
Moffett Field, CA, USA

Mark B. Tischler[1]
Senior Technologist
U.S. Army DEVCOM
Aviation & Missile Center
Moffett Field, CA, USA

Christina M. Ivler
Assistant Professor of Mechanical Engineering
Shiley School of Engineering
University of Portland
Portland, OR, USA

ABSTRACT

The control equivalent turbulence input (CETI) modeling approach uses flight data taken in turbulence and identifies control inputs that would effectively reproduce the aircraft's response to turbulence. CETI models are extracted and presented for a quad-, hexa- and octocopter using flight test data collected in different wind conditions. Time domain simulation of the developed turbulence models is verified with flight test data. The effects of wind intensity are studied by comparing extracted turbulence models against the collected wind information. The effects of output measurement noise on CETI model identification are studied in simulation as well. The implications of these findings are discussed in relation to the development of a reconfigurable CETI model for multirotor UAS.

INTRODUCTION

Multirotor unmanned aerial systems (UAS) have grown increasingly popular across a variety of military and commercial applications. Within the military, multirotor UAS are being developed for surveillance, reconnaissance, and resupply missions. For commercial use, multirotor UAS are being developed as package delivery drones and for urban air mobility applications. Due to their wide range of applications, multirotor UAS are incredibly versatile. Their versatility is partly due to their ability to precisely hover and maneuver through dense environments, while often subject to windy and turbulent flight conditions. The flight control system's disturbance rejection capabilities must be properly designed and evaluated to ensure adequate performance in these adverse conditions. A realistic turbulence model can be used in simulation to effectively tune and evaluate control system performance.

Several sources have shown the success of a frequency-domain based turbulence modeling framework that relies on a control equivalent turbulence input (CETI) model. In the CETI modeling approach, flight data taken in turbulence is used to identify a model that generates control inputs that would reproduce the aircraft's response to turbulence. The CETI approach was first used in the development of turbulence models for the UH60 helicopter (Ref. 1). In that work, a white noise driven mixer equivalent turbulence simulation model was used to produce realistic turbulence effects at low speed and hover conditions for the UH60 helicopter. Since then, the CETI modeling methodology has been used and validated to accurately predict the turbulence response of a quadrotor, hexacopter, octocopter and tail sitter UAS (Refs. 2-5). Juhasz, et al. examined the effects of signal length, feedback noise, and model uncertainty on the extraction methodology and subsequently provides a set of guidelines to ensure accurate CETI model extraction (Ref. 2). In another work, Juhasz, et al. developed a CETI model for a tail-sitter UAS using flight data taken in various turbulence levels (Ref. 3). Lopez, et al. identified CETI models for a quad-, hexa-, and octocopter and used them to physically simulate turbulence in flight to assess gust rejection performance (Ref. 4). Berrios, et al. similarly identified CETI models for a quadcopter to simulate turbulence in flight and

---

[1] Retired from US Army; currently, Tischler Aeronautics

assess optimized control laws for gust rejection capabilities. In these works, the extracted turbulence models were successfully applied to flight control design to improve gust rejection performance.

Following the developments of Ref. 1, a reconfigurable turbulence model for conventional helicopters was successfully developed using the CETI approach (Ref. 6). The model consisted of white noise driven filters based on Dryden spectral models of atmospheric turbulence. This model is scalable with wind speed and turbulence intensity. It is presumed that a similar approach can be adapted for multirotor UAS. Hence, this research effort is motivated by the development of a reconfigurable turbulence model for multirotor UAS based on a database of empirical models.

The work presented in this paper builds off previous turbulence modeling efforts and presents CETI models for three different multirotor UAS. CETI models are extracted using flight test data collected at two wind condition levels. Consistent with Refs. 2-5, the developed CETI models are validated in simulation against flight data in turbulence. This work provides a better understanding of the CETI modeling method as well as the effects of wind intensity on CETI modeling. This paper contributes to the development of a reconfigurable turbulence model by providing validated CETI models for three different multirotor UAS at a moderate and low wind condition.

The paper is arranged as follows. First, the flight test methodology is discussed, including a description of the three test vehicles. Next, the CETI extraction method and formulation is presented. Then, the identified CETI models are shown alongside validation results. Finally, a discussion of the results of the paper and conclusions is provided.

FLIGHT TEST METHODOLOGY

Test Vehicles Description

Flight testing was performed for the collection of turbulence data for the Technology Development Directorate (TDD) quad-, hexa- and octocopter. The three different multirotor configurations were constructed with common parts with differences only in the number and location of arms and rotors. The work herein uses stock control systems from Arducopter for data collection. Vehicle mass and size properties can be found in Table 1. Images of the flight vehicles can be found in Figure 1.

Table 1. Test Vehicle Properties

Property	Quadcopter	Hexacopter	Octocopter
Rotor Diameter (in)	18	18	18
Hub-to-hub Distance (in)	50	50	50
Weight (lb)	13.4	15.7	18.1
I_{xx} (lb-ft^2)	7.7	11.2	14.7
I_{yy} (lb-ft^2)	7.8	11.3	14.9
I_{zz} (lb-ft^2)	14.7	21.7	28.6

(a) Quadcopter

(b) Hexacopter

(c) Quadcopter

Figure 1. Images of each multirotor vehicle

Wind Information

In recent flight testing, wind speeds and turbulence levels were quantified by an ultrasonic anemometer, shown in Fig. 2. The anemometer was capable of recording wind speeds and direction for the entire flight test duration. The flight-testing set-up can be found in Fig 3. Wind speeds were recorded along the x, y, and z axes at vehicle level. Wind direction and elevation were recorded as well. Sample anemometer information can be found in the flight data section.

Figure 2. Anemometer

Figure 3. Flight Testing Set-up

Flight Data

Flight data collection took place in June 2018 and December 2020. On both days, all three multirotor vehicles were flown at a hover flight condition and turbulence data was collected in the longitudinal, lateral, pedal, and collective axis. Long (approximately 300 sec) time histories were collected to ensure that the aircraft response to turbulence and low frequency dynamics were adequately captured. Flight test procedures were consistent with the CETI extraction guidelines described in Ref. 3. A summary of the flight data can be found in Table 2.

Table 2. Flight Data Summary

Flight Date	Vehicle	Anemometer Information	Total Flight Time (sec)
June 2018	Quadcopter		363
	Hexacopter	No	609
	Octocopter		385
December 2020	Quadcopter		276
	Hexacopter	Yes	290
	Octocopter		266

In data from June 2018, the average wind speed was recorded at 10 MPH using local weather stations. In data from December 2020, average wind speed was recorded at 2 MPH using an on-site ultrasonic anemometer. Anemometer data from this flight data can be found in Table 3. For the remainder of the paper, the flight data collected in 2018 and 2020 will be referred to as moderate and low wind data, respectively.

Table 3. Anemometer Data, December 2020

Anemometer (MPH)	Quadcopter	Hexacopter	Octocopter
Average U	1.71	2.35	1.81
Average V	2.49	2.16	2.41
Average W	0.25	0.24	0.27
RMS U	1.85	2.42	1.99
RMS V	2.55	2.36	2.54
RMS W	0.41	0.35	0.43

CETI METHOD AND FORMULATION

Extraction Methodology

The CETI approach identifies equivalent control inputs that excites the aircraft in a similar way as real turbulence. This concept is shown in block diagram form in Fig. 4, where the measured aircraft response (y) is driven by the sum of the commanded input (x) and turbulence input (n). H is the aircraft bare-airframe transfer function from control input u to output y. The turbulence input (n) is generated by passing white noise (w) through the CETI transfer function T.
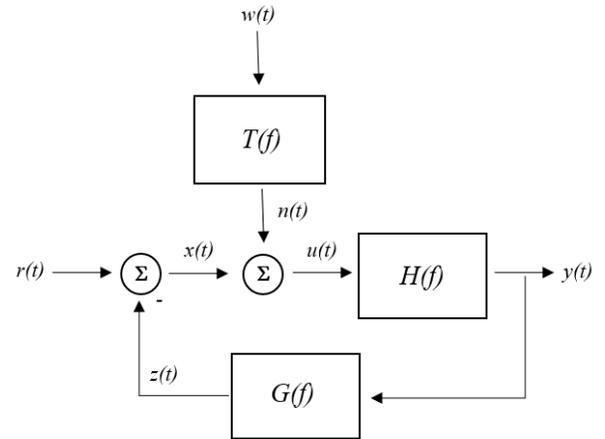
Figure 4. CETI Block Diagram

In equation form, the measured aircraft response is given in the frequency domain as:

$$Y(f) = H(f) \ [X(f) + N(f)] \qquad (1)$$

Solving for the turbulence input gives:

$$N(f) = \frac{1}{H(f)} Y(f) - X(f) \qquad (2)$$

From here, the equation is multiplied by its complex conjugate (Ref. 7):

$$NN^* = \frac{1}{H_{xy}H^*_{xy}} YY^* - \frac{1}{H_{xy}} YX^* - \frac{1}{H^*_{xy}} Y^*X \\ + XX^* \qquad (3)$$

This provides the auto- and cross-spectra form of an estimate of G_{nn}:

$$\widehat{G}_{nn} = \frac{1}{|H_{xy}|^2} G_{yy} - \frac{1}{H_{xy}} G_{xy} - \frac{1}{H^*_{xy}} G_{yx} + G_{xx} \qquad (4)$$

Finally, the equation can be simplified to the following form:

$$\widehat{G}_{nn} = \frac{1}{|H_{xy}|^2} G_{yy} + G_{xx} - 2\mathrm{Re}\left(\frac{G_{xy}}{H_{xy}}\right) \qquad (5)$$

Note that the equation for $\widehat{G}_{nn}$ developed here is different from that used in Ref. 2, as it accounts for the correlation of the aircraft control input *u* and output *y* due to the feedback.

Bare-Airframe System Identification Models

Bare-airframe models for the quad-, hexa- and octocopter have been previously identified in system identification

efforts in Ref. 5. The block diagram used in system identification is shown in Fig. 5. The identified bare airframe Q had individual actuators as inputs in units of PWM while the CETI approach's bare-airframe model H uses non-dimensional mixer input signals. Therefore, an effective mixer K was identified to produce the effective bare-airframe H, a mixer input model, for use in the CETI extraction formula.
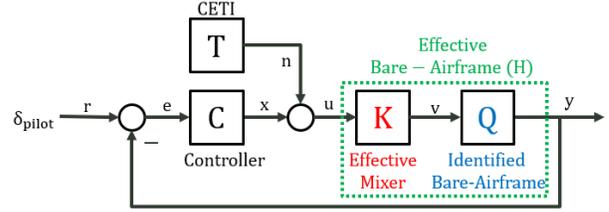
Figure 5. Bare-Airframe System Identification

CETI MODEL EXTRACTION USING FLIGHT DATA

Identification Methodology

The CETI method was used to identify turbulence models for the TDD quad-, hexa- and octocopter vehicles using CIFER® (Ref. 8). Turbulence models were identified using the low wind and moderate wind flight data separately. A first-order transfer function was identified from the CETI data to form turbulence models for the longitudinal, lateral, pedal and collective axes. All identified CETI models for both wind conditions are shown in Table 4. Non-dimensional units were used throughout the CETI derivation to simplify future reconfiguration. These signals included the mixer inputs (+1/-1) and the measured aircraft rates (rad/sec).

The first-order transfer function model and the PSD data used

Table 4. Identified CETI Models

Vehicle	Wind Level	Longitudinal CETI Model	Lateral CETI Model	Pedal CETI Model	Collective CETI Model
Quadcopter	Moderate	$\dfrac{0.0075}{s + 0.17}$	$\dfrac{0.011}{s + 0.24}$	$\dfrac{0.13}{s + 3.4}$	$\dfrac{0.015}{s + 1.1}$
	Low	$\dfrac{0.0024}{s + 0.087}$	$\dfrac{0.0027}{s + 0.17}$	$\dfrac{0.039}{s + 5.3}$	$\dfrac{0.0014}{s + 0.26}$
Hexacopter	Moderate	$\dfrac{0.0062}{s + 0.062}$	$\dfrac{0.012}{s + 0.65}$	$\dfrac{0.037}{s + 0.98}$	$\dfrac{0.0056}{s + 0.59}$
	Low	$\dfrac{0.0026}{s + 0.012}$	$\dfrac{0.0045}{s + 0.027}$	$\dfrac{0.014}{s + 0.95}$	$\dfrac{0.0027}{s + 0.51}$
Octocopter	Moderate	$\dfrac{0.012}{s + 0.13}$	$\dfrac{0.014}{s + 0.24}$	$\dfrac{0.053}{s + 2.0}$	$\dfrac{0.0096}{s + 0.84}$
	Low	$\dfrac{0.0029}{s + 0.032}$	$\dfrac{0.0033}{s + 0.049}$	$\dfrac{0.016}{s + 0.57}$	$\dfrac{0.0024}{s + 0.47}$

in the CETI identification are shown for the longitudinal axis in Fig. 6 for all test vehicles. The plotted lines are color coordinated to distinguish between the low wind (blue) and moderate wind (black) flight data sets. The solid lines represent the CETI PSD extracted using the CETI method (Eq. 5). The dashed lines represent the first-order transfer function model that was identified using CIFER®. Model fits were made at lower frequencies, less than 1 rad/sec, with a maximum model cost $J = 65$, which is within the adequate range for reliable model fits (Ref. 8). The frequency range used for model fitting is discussed and explained further in a later section.
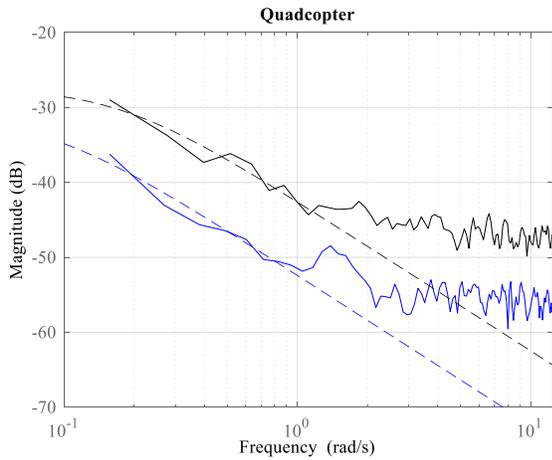
(a) Quadcopter
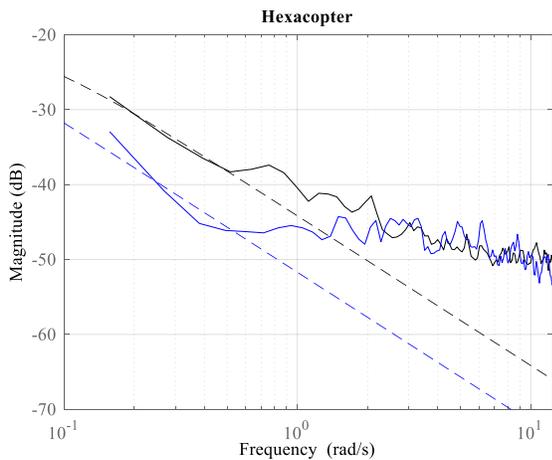
(b) Hexacopter
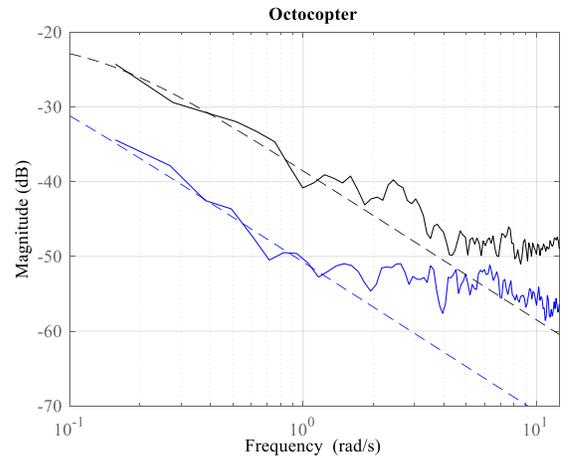
(c) Octocopter
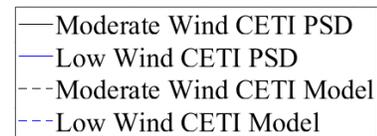
Figure 6. Longitudinal CETI PSD and Models

Validation

Time domain validation is conducted using an open-loop simulation in the collective axis, which is shown in block diagram form in Fig. 7. The collective axis is used here because it is the only stable axis in hover, which can be simulated open loop. The CETI transfer function T used in simulation was the first order transfer function model identified in CETI extraction. H is the aircraft effective bare-airframe transfer function from control input u to output y. Additionally, measurement noise, $m(t)$, is summed in at the output to account for the effects of output measurement noise in CETI extraction. For the collective axis, the simulated aircraft rate is vertical acceleration.
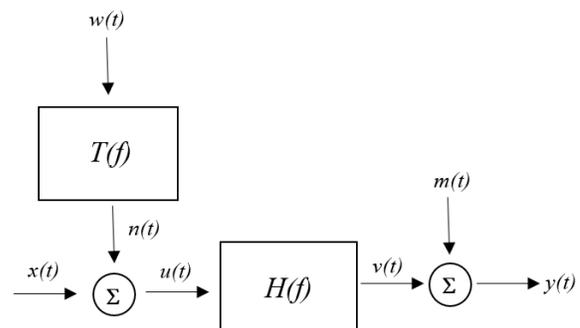
Figure 7. Open-Loop Validation Block Diagram

Time domain validation of the quadcopter's collective axis CETI models is shown in Fig. 8 and Fig. 9 by comparing time

5

histories from flight data with aircraft in turbulence versus simulation with aircraft excited by the CETI model. For both time histories, the aircraft response is entirely due to turbulence and output measurement noise due to the absence of commanded inputs. Since the CETI identification process is unable to capture the high frequency dynamics of flight data, the low order form CETI model in simulation is unable to reproduce the high frequency content seen in flight data. Due to this, both time histories were filtered using a second order filter at 20 rad/sec, well above the range of identification. This filtering enables the comparison between actual flight data and the simulated data without high frequency content.

Overall, both time domain validations show an excellent qualitative agreement with the flight data. Quantitatively, the root mean square (RMS) values for both validations are on the same order of magnitude. For the moderate wind CETI model verification, in Fig. 8, the RMS value for the simulated CETI response is 0.26 while the RMS value for the actual turbulence response is 0.30. Additionally, for the low wind CETI model verification, in Fig. 9, the RMS value for the simulated CETI response is 0.067 while the RMS value for the actual turbulence response is 0.071. The CETI model simulated response to turbulence has similar oscillations to the flight data. It is not expected for the flight data and simulation time histories to perfectly line up due to the random nature of turbulence, only that they have similar amplitudes of oscillation.

.
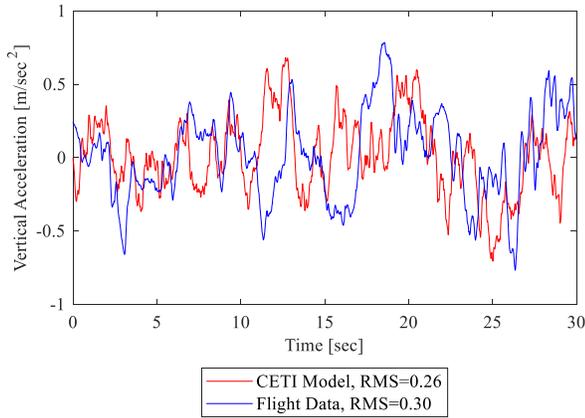
Figure 8. Moderate Wind CETI Model Verification
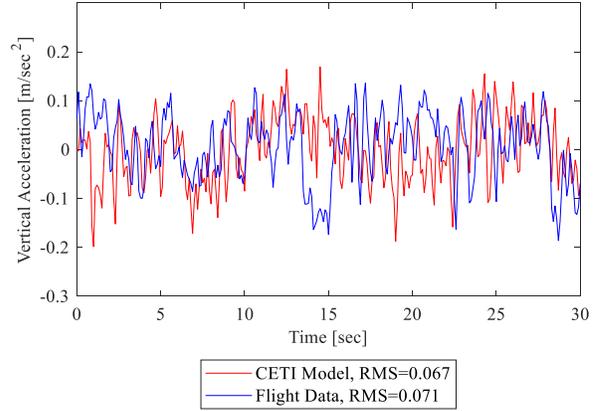
Figure 9. Low Wind CETI Model Verification

DISCUSSION

Effects of Output Measurement Noise

In CETI extraction, it is assumed that there is no output noise, hence there are no noise terms in Eq. 5. This is due to the fact that there are no independent measurements of the measurement noise in actual flight data. The time domain validation accounts for output measurement noise by summing in simulated measurement noise, *m(t)*, as seen in Fig. 7. Following the block diagram depicting the open loop case, the CETI identification equation then becomes:

$$\widehat{G}_{nn} = \frac{1}{|H|^2}\left(G_{yy} - G_{ym} - G_{my} + G_{mm}\right) \tag{6}$$
$$+ \frac{1}{H}\left(G_{mx} - G_{yx}\right)$$
$$+ \frac{1}{H^*}\left(G_{xm} - G_{xy}\right) + G_{xx}$$

Since the validation is open loop and x(t)=0, the equation reduces to:

$$\widehat{G}_{nn} = \frac{1}{|H|^2}\left(G_{yy} + G_{mm} - 2\text{Re}\left(G_{my}\right)\right) \tag{7}$$

Ignoring measurement noise, like in CETI extraction shown in Eq. 5, Eq. 7 simplifies to:

$$\widehat{G}_{nn} = \frac{1}{|H|^2}\left(G_{yy}\right) \tag{8}$$

6

This demonstrates that when ignoring measurement noise, there will be a bias in the identified CETI PSD $\widehat{G}_{nn}$ given by:

$$\widehat{G}_{nn_{bias}} = \frac{1}{|H|^2}\left(G_{mm} - 2\text{Re}(G_{my})\right) \qquad (9)$$

A simulation study, using the open loop validation in the collective axis, was used to see the effects of output measurement noise on CETI extraction. This is achieved by using the identified CETI models in simulation with and without the addition of measurement noise and re-extracting a CETI model using the simulated data. CETI model extraction was performed with and without measurement noise in simulation to address the validity of the assumptions made in Eq. 5. The results from this case study are shown in Fig. 10.

In Fig. 10, the dashed black line is the PSD extracted from flight data. The red line is the PSD extracted using Eq. 8 with a constant noise power of 0.03 in simulation. This amount was consistent with the high frequency gain of the output autospectra. The orange line is the PSD extracted when no output noise is added to the system. Finally, the blue line is the CETI transfer function model identified from flight data and used in simulation.

In Fig. 10a, the PSD extracted in simulation assuming that there is no output measurement noise fails to track the CETI transfer function model but aligns with the PSD extracted from flight data after 1 rad/sec. This suggests that the reason the flight data PSD flattens out after 1 rad/sec is because of output measurement noise. The flattening effect this assumption has is less prominent in the moderate wind PSDs, in Fig. 10b. This is likely due to the greater aircraft excitation experienced at the moderate wind condition (greater CETI signal to measurement noise ratio).
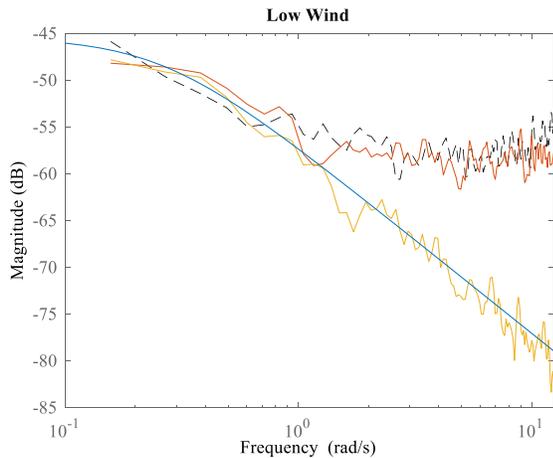
(a) Low Wind
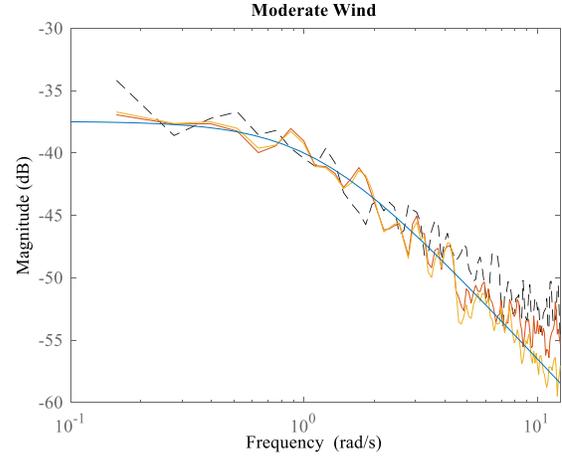
(b) Moderate Wind
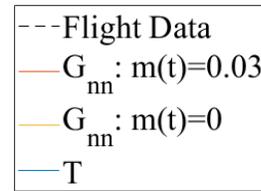
Figure 10. Output Measurement Noise Effects on CETI PSD

Effects of Wind Intensity on CETI Models

Consistently across all test vehicles and control axes, there is a significant difference in gain when comparing between CETI models extracted using the moderate wind data versus the low wind data. As an example, the extracted CETI models for the quadcopter are shown in Fig. 11. Additionally, all identified CETI models in the longitudinal axis are overlayed in Fig. 12. The CETI models extracted using the moderate wind data consistently have higher gain than models extracted from the low wind data. This suggests that the observed difference in gain is proportional to the difference in wind speeds. The same trend is not evident when comparing the break frequencies of the two different sets of extracted CETI models. When comparing between the different control axes, there are similar gain differences between the longitudinal and lateral models which is expected due to vehicle symmetry.
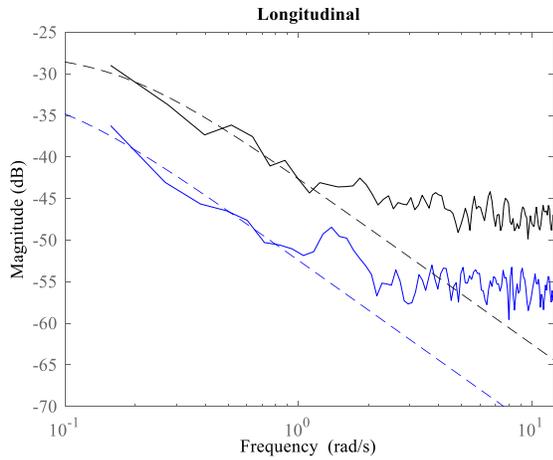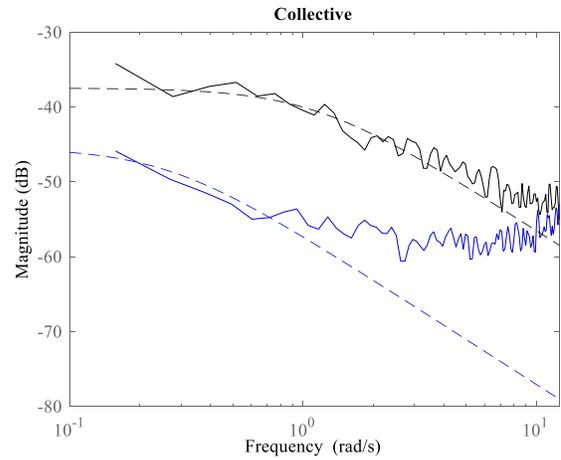
(a) Longitudinal CETI

(b) Lateral CETI
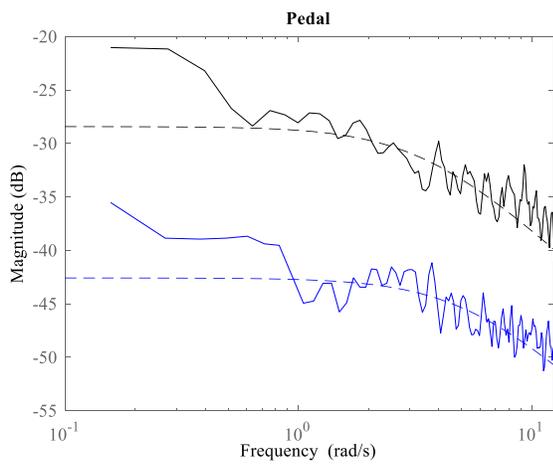
(c) Pedal CETI

(d) Collective CETI
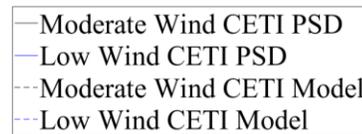
Figure 11. Quadcopter CETI Models
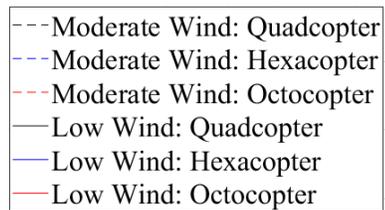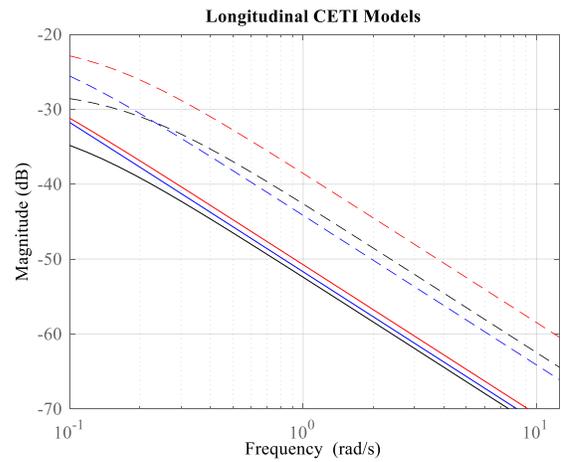
Figure 12. Longitudinal CETI Models

8

TOWARDS A RECONFIGURABLE CETI MODEL FOR MULTIROTOR UAS

All extracted CETI models in this work shared a similar characteristic first order form at low frequencies, seen in Eq. 10. The extracted CETI models from the moderate wind and low wind data set showed a correlation between wind intensity and model gain. This suggests that wind speed can potentially be used to scale CETI model gain, K. From the results presented here, there is not a clear relationship between wind intensity and model break frequency, a. Additional flight data is needed to expand the database before scale factors and reconfiguration can be considered.

$$G_{\delta_t}(s) = \frac{K}{s + a} \qquad (10)$$

In future work, additional CETI models should be identified at different wind conditions. Considering the effects of output measurement noise, it is suggested that model fits be made at lower frequency ranges when flight data is collected at lower wind conditions. Flight data collected in more turbulent conditions can provide more information at higher frequencies since they are less susceptible to the effects of output measurement noise when compared against data collected in ambient conditions. An anemometer is recommended as well as it provides thorough wind information and helps quantify the effects of wind intensity. Once additional CETI models have been identified at new wind speeds, a database of all models and wind information can be used to determine scaling factors needed for CETI model reconfiguration.

CONCLUSIONS

The work herein presented and validated turbulence models for a quad-, hexa-, and octocopter UAS using the control equivalence turbulence input modeling method. Models were extracted at two different wind conditions: moderate wind and low wind speeds. The key conclusions from this paper are:

1. The CETI modeling method has been shown and validated to be effective in producing realistic turbulence models from flight data.
2. Thorough wind information is needed to identify scaling factors needed for the development of a reconfigurable CETI model.
3. The extracted CETI model gain is dependent on wind speeds experienced during flight data collection.
4. Output measurement noise can have a distorting effect on extracted CETI PSDs at higher frequencies. Flight data collected in more turbulent conditions is less susceptible to the distortion caused by output measurement noise when compared against flight data collected in more ambient conditions.

REFERENCES

1. Lusardi, J. A., Blanken, C. L, Tischler, M. B., "Piloted Evaluation of a UH-60 Mixer Equivalent Turbulence Simulation Model," AHS 59th Annual Forum, Phoenix, AX, May 6-8, 2003.

2. Juhasz, O., Lopez, M. J. S., Berrios, M. G., Berger, T., and Tischler, M. B., "Turbulence Modeling of a Small Quadrotor UAS using System Identification from Flight Data," Seventh AHS Technical Meeting on VTOL Unmanned Aircraft Systems, Mesa, AZ, January 24-26, 2017.

3. Juhasz, O., Tischler, M. B., and Won, H., "System Identification and Control Law Optimization Applied to the AeroVironment QuantixTM Tail-Sitter UAS," AHS International 74th Annual Forum & Technology Display, Phoenix, AZ, May 14-17, 2018.

4. Lopez, M. J. S., Tischler, M. B., Juhasz, O., Gong, A., Sanders, F. C., Soong, J. Y., Nadell, S. J., "Flight Test Comparison of Gust Rejection Capability for Various Multirotor Configurations," VFS 75th Annual Forum & Technology Display, Philadelphia, PA, May 13-16, 2019.

5. Berrios, M.G., Berger, T., Tischler, M. B., Juhasz, O., and Sanders, F. C., "Hover Flight Control Design for UAS Using Performance-based Disturbance Rejection Requirements," AHS International 73rd Annual Forum & Technology Display, Fort Worth, TX, May 9-11, 2017.

6. Lusardi, J. A., Tischler, M. B., Blanken, C. L., "Empirically Derived Helicopter Response Model and Control System Requirements for Flight in Turbulence," *Journal of the American Helicopter Society*, Volume 49, Number 3, July 2004, pp. 340-349.

7. Bendat, J. S. and Piersol, A. G., *Random Data: Analysis and Measurement Procedures*, 2nd ed., Wiley, New York, 1986.

8. Tischler, M. B. and Remple, R. K., *Aircraft and Rotorcraft System Identification: Engineering Methods with Flight Test Examples*, 2nd ed, AIAA, Reston, VA, 2012.